IEEE Access
Multidisciplinary | Rapid Review | Open Access Journal

Received 2 December 2022, accepted 12 December 2022, date of publication 20 December 2022,
date of current version 23 February 2023.

Digital Object Identifier 10.1109/ACCESS.2022.3231106

RESEARCH ARTICLE

The Rough Prototype and Fine Tuning (RP-FT) Method for Multiband Bandpass Filter Synthesis

RIHAN WU[1], (Member, IEEE), JUNLING HE[1], XIAOHONG TANG[1], (Member, IEEE), ZONGQI CAI[2], LIKANG XIAO[1,3], AND FEI XIAO[1], (Member, IEEE)

[1]School of Electronic Science and Engineering, University of Electronic Science and Technology of China (UESTC), Chengdu, Sichuan 610054, China
[2]National Key Laboratory of Science and Technology on Reliability Physics and Application of Electronic Component, China Electronic Product Reliability and Environmental Testing Research Institute, Guangzhou 510610, China
[3]Southwest Institute of Applied Magnetics, Mianyang 621000, China

Corresponding authors: Zongqi Cai (zqcai.uestc@hotmail.com), Likang Xiao (xiaolikang@cetc.com.cn), and Fei Xiao (fxiao@uestc.edu.cn)

This work was supported by the National Natural Science Foundation of China under Project 61671111.

ABSTRACT Nowadays, various new communication technologies operating in different frequency bands emerge constantly. There is a trend to integrate more than one of them into single system, for optimizing whole system performance and volume. As an important circuit component for frequency selection, the research on multiband bandpass filter (MB-BPF) receives much attention. This paper proposes a novel synthesis method for MB-BPF. It applies two frequency transformations on the specifications of the MB-BPF to be synthesized, so that a rough prototype containing the information of transmission and reflection zeros is constructed first. Then, optimization is applied for fine tuning until equal ripples are achieved in each passband. For simplicity, it is called the Rough Prototype and Fine Tuning (RP-FT) method, which demonstrate great advantage in flexibly controlling the performance of a MB-BPF such as passband number, performance of each passband, transmission zeros, etc. Furthermore, the filtering polynomials derived by the RP-FT method could be transformed into specific coupling matrixes for physical realization. For illustration, this paper derives a specific coupling matrix form, and applies it in the design of a microstrip quad-band bandpass filter. The measurement well verifies the validity of design process.

INDEX TERMS Coupling matrix, frequency transformation, filtering polynomial, multiband bandpass filter (MB-BPF), rough prototype and fine tuning (RP-FT) method.

I. INTRODUCTION

Recently, various communication technologies, such as GPRS, WCDMA, TD-SCDMA, LTE-Advanced, WIFI, WiMAX and others, have emerged constantly. Integrating multiple technologies in single system is becoming a trend, in order to optimize system performance and volume. For the sake of limited spectrum resource, the operation bands of some technologies are close. It is necessary to develop multi-band bandpass filter (MB-BPF) for frequency selection.

Up to now, some effort has been made on the synthesis method of MB-BPF. For example, [1], [2], [3], and [4] propose some frequency transformation relations to map a lowpass response to a multiband bandpass one, and then obtain the filtering polynomials constituting the scattering parameters. [5] constructs the characteristic function of each passband independently at first, and then sums up the reciprocals of all the characteristic functions to form the characteristic function of MB-BPF. Meanwhile, [6] and [7] do it through multiplying the characteristic functions of all the passbands. Reference [8], [9], [10], [11], [12], and [13] utilize optimization to obtain the filtering polynomials. In [8] and [9] the old transmission zeros or reflection zeros are exchanged one by one, so that the new ones can make the ripples in the passband or the stopband more equal. Reference [10], [11], and [12] solve the Zolotarev problem according to the criterion that the modulus of the transmission is as big as possible

The associate editor coordinating the review of this manuscript and approving it for publication was Photos Vryonides.

in the passbands and as small as possible in the stopbands. Reference [13] iteratively updates the critical points until the value of the characteristic function at these points meet expectation. However, some will face some problems such as the limited freedom of setting return loss or transmission zeros of each passband. In addition, the ripples might be unequal in passband. In addition, there are also some nice works on physical realization of MB-BPF, such as [14], [15], [16], [17], [18], [19], [20], [21], [22], [23], [24], [25], [26], [27], [28], [29].

In this paper, a new synthesis method named the RP-FT method is proposed for MB-BPF. In order to accelerate design process, it utilizes a hybrid approach. The analytic part plays an important role in determining key information such as transmission and reflection zeros, so that a rough prototype is easily set up. Such will greatly alleviate strict requirement on next step. Then, optimization-based fine tuning is applied to achieve equal ripples in all passbands by introducing extra transmission zeros (ETZs) and shifting the positions of reflection zeros. The RP-FT method can efficiently derive filtering polynomials. Based on those, various coupling matrices could be obtained for practical realization. Especially, a L-branch folded topology is discussed. Finally, a microstrip quad-band bandpass filter corresponding to the 4-branch folded topology is designed, fabricated and measured for verification.

The whole paper is organized as follows. Section II discusses how to use the RP-FT method to derive filtering polynomials in detail. In Section III, a general approach to transform transverse coupling matrix into a specific form corresponding to L-branch folded topology is discussed, and then the quality factors and the coupling coefficients are obtained for use. For demonstration, a quad-band bandpass filter example is synthesized by the RP-FT method in Section IV. Its filtering polynomials are obtained, the coupling matrix for the 4-branch folded topology is derived, and then the design parameters such as the quality factors and the coupling coefficients are obtained. Section V presents a microstrip realization corresponding to the 4-branch folded topology and measurement, which effectively verifies the proposed RP-FT method. Finally, the conclusion is drawn in Section VI.

II. FILTERING POLYNOMIAL SYNTHESIS

As a two-port network component, an analogue filter can be described by scattering parameters. For example, S_{21} and S_{11} are expressed as rational fractions in terms of the complex frequency variable s.

$$S_{21}(s) = \frac{P(s)}{E(s)} \tag{1}$$

$$S_{11}(s) = \frac{F(s)}{E(s)} \tag{2}$$

where $P(s)$, $F(s)$ and $E(s)$ are the transfer polynomial, the reflection polynomial, and the common polynomial, respectively. For the synthesis of a MB-BPF, it is not easy to derive these scattering parameters directly in the bandpass frequency domain (denoted as the f-domain in this paper). Thus, we apply two frequency transformations on the specifications of the MB-BPF to be synthesized, so that the synthesis is done in the multi-band normalized frequency domain (denoted as the Ω-domain). In other words, $s = j\Omega$. Then, these polynomials can be expressed as

$$P(j\Omega) = \frac{1}{\varepsilon}\prod_{m=1}^{M}(j\Omega - j\Omega_m) \tag{3}$$

$$F(j\Omega) = \prod_{n=1}^{N}(j\Omega - j\Omega_n) \tag{4}$$

$$E(j\Omega)\cdot E(j\Omega)^* = P(j\Omega)\cdot P(j\Omega)^* + F(j\Omega)\cdot F(j\Omega)^* \tag{5}$$

Suppose that there are M transmission zeros at finite frequency and the mth one is denoted as $j\Omega_m$. There are N reflection zeros, and the nth one is denoted as $j\Omega_n$. ε is the ripple coefficient. In addition, the characteristic function is defined as [30]

$$K(j\Omega) = \frac{F(j\Omega)}{P(j\Omega)} \tag{6}$$

This section focuses on how to derive these filtering polynomials in detail.

The proposed RP-FT method is a hybrid approach, in which a rough prototype of the MB-BPF is obtained firstly and then fine tuning is applied until equal ripples are achieved in each passband. To obtain the rough prototype, each passband of the MB-BPF is regarded as a single-band bandpass filter, and then is synthesized separately to determine their reflection zeros. By using the specified transmission zeros and the reflection zeros, the rough prototype of the MB-BPF is constructed. Next, in the process of the fine tuning, extra transmission zeros (ETZs) are introduced and the positions of the reflection zeros are shifted, so that equal ripples in each passband can be achieved. The design flowchart of the RP-FT method is shown in Figure 1.

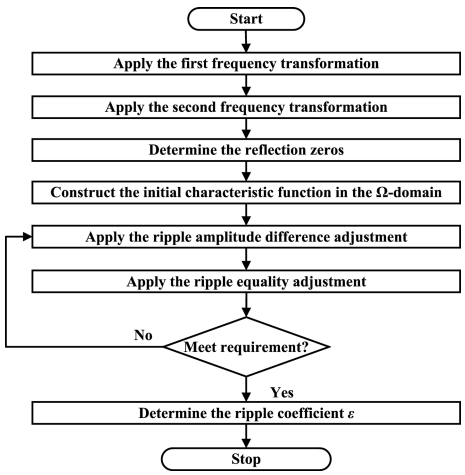

FIGURE 1. Design flowchart of the RP-FT method.

Step 1 (Apply the First Frequency Transformation): Suppose that the MB-BPF to be synthesized has L passbands. Its

specifications are given in the f-domain, such as the number L of the passbands, the order Od_l, the return loss RL_l, the lower edge frequency jf_{ld}, the upper edge frequency jf_{lu}, the specified transmission zeros $jf_{T,lm}$ of each passband, etc. The subscript l represents the lth passband where $l = 1, 2, \ldots,$ and L. The subscript m represents the mth transmission zero assigned to the lth passband. In the process of deriving the rough prototype, each passband of the MB-BPF is regarded as single-band bandpass filter. Therefore, each specified transmission zero will be assigned to one passband according to its location.

We apply the first frequency transformation to transform the key information such as the edge frequencies and the specified transmission zeros from the f-domain to the Ω-domain.

$$\Omega = \frac{2\pi\ (f - f_0)}{scale} \tag{7}$$

where $f_0 = (f_{1d} + f_{Lu})/2$ is the center frequency of the total frequency range that the whole passband of the MB-BPF covers. $Scale{=}2\pi\,(f_{Lu} - f_{1d})/2$ is called the scaling factor. The first frequency transformation is illustrated in Figure 2. It will transform the total frequency range $[f_{1d}, f_{Lu}]$ of the MB-BPF in the f-domain to $[-1, 1]$ in the Ω-domain.

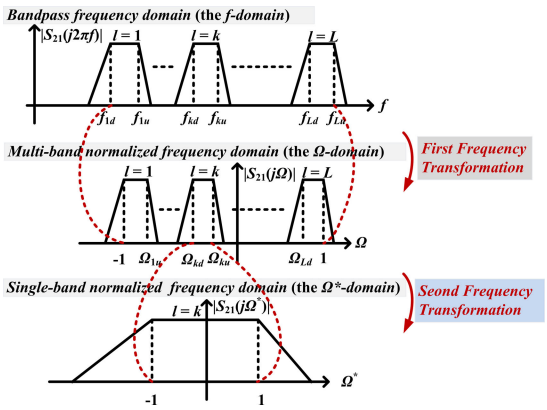

FIGURE 2. Two frequency transformations.

Step 2 (Apply the Second Frequency Transformation): After the first frequency transformation, the specifications of the MB-BPF are transformed to those in $[-1, 1]$ in the Ω-domain. Subsequently, we apply the second frequency transformation on the specifications of each passband to the Ω^*-domain.

$$\Omega_l^* = \frac{\Omega - \Omega_{l0}}{scale_l^*}, \quad l = 1, 2, \ldots, L \tag{8}$$

where $\Omega_{l0} = (\Omega_{ld} + \Omega_{lu})/2$ is the center frequency of the lth passband, and $scale_l^* = (\Omega_{lu} - \Omega_{ld})/2$ is the scaling factor of the lth passband. The second frequency transformation is illustrated in Figure 2. It will transform the frequency range of each passband $[\Omega_{ld}, \Omega_{lu}]$ in the Ω-domain to $[-1, 1]$ in the Ω^*-domain. Then, the specified transmission zeros of each passband can be obtained in the Ω^*-domain, and the order of each passband is also known.

Step 3 (Determine THE Reflection Zeros): After the second frequency transformation, the specifications of each passband in the Ω^*-domain can be regarded as those of a single-band bandpass filter, and then conventional single-band bandpass filter synthesis technique can be applied to synthesize each passband [30]. Accordingly, the reflection zeros of each passband can be obtained. Then, by using Eq. (8), these reflection zeros can be transformed back to the Ω-domain. Thus, both the specified transmission zeros and the reflection zeros of the MB-BPF are known in the Ω-domain.

Step 4 (Construct the Initial Characteristic Function of the MB-BPF): By multiplying the characteristic functions of each passband of the MB-BPF in the Ω-domain, the initial characteristic function of the MB-BPF is written as

$$K_0(j\Omega) = \prod_{l=1}^{L} \frac{\prod_{n=1}^{N_{R,l}} (j\Omega - j\Omega_{R,ln})}{\prod_{m=1}^{M_{T,l}} (j\Omega - j\Omega_{T,lm})} \tag{9}$$

where $j\Omega_{R,ln}$ is the nth reflection zero and $j\Omega_{T,lm}$ is the mth specified transmission zeros of the lth passband. The number of the reflection zeros and the specified transmission zeros of the lth passband are $N_{R,l}$ and $M_{T,l}$, respectively.

Unfortunately, there is a problem with $K_0(j\Omega)$, i.e., the ripples in each passband might not be equal. Here, two measures are utilized for achieving the required level of the ripples. Firstly, some ETZs are introduced to adjust the ripple amplitude difference between different passbands. This measure is called the ripple amplitude difference adjustment. Secondly, the reflection zeros are shifted to achieve the ripple equality, which is called the ripple equality adjustment.

Step 5 (Apply the Ripple Amplitude Difference Adjustment): In order to evaluate the ripple amplitude difference among different passbands, an index named the estimated ripple amplitude (ERA) denoted as U_l is defined as

$$U_l = \frac{20\lg|K_0\,(j\Omega_{lu})| + 20\lg|K_0\,(j\Omega_{ld})|}{2} + \Delta R_l \tag{10}$$

In general case, the MB-BPF might be specified to have different return loss in each passband. Then, ΔR_l represents the difference between the return loss of the lth passband and the maximum return loss among the ones of all passbands. For the MB-BPF with L passbands, Eq. (10) is used to calculate the ERA of each passband, i.e., U_l $(l = 1, 2, \ldots, L)$. If the maximum one of these ERAs is denoted as $U_{\max}$, then the ripple amplitude difference of each passband is defined as ΔU_l, i.e.,

$$\Delta U_l = U_{\max} - U_l \tag{11}$$

ΔU_l represents the value of the ripple amplitude to be compensated for the lth passband.

To adjust the ripple amplitude difference, some ETZs need to be introduced. For example, the ith ETZ is denoted as $j\Omega_{E,i}$. Then, a modified characteristic function denoted as K_E is

defined as

$$K_E(j\Omega) = \prod_{l=1}^{L} \frac{\prod_{n=1}^{N_{R,l}} \left(j\Omega - j\Omega_{R,ln}\right)}{\prod_{m=1}^{M_{T,l}} \left(j\Omega - j\Omega_{T,lm}\right)} \prod_{i=1}^{I} \frac{1}{\left(j\Omega - j\Omega_{E,i}\right)} \tag{12}$$

If the concept of Decibel is applied, then

$$K_E\,(dB) = K_0\,(dB) + \sum_{i=1}^{I} 20\lg\left(\frac{1}{\left|j\Omega - j\Omega_{E,i}\right|}\right) \tag{13}$$

The second term in Eq. (13) represents the effect of the ETZs, which can be used to adjust the ripple amplitude difference among different passbands. For illustration, the response of $20\lg(1/|j\Omega - j\Omega_{E,i}|)$, is shown in Figure 3. When Ω approaches to $\Omega_{E,i}$, the function value will increase sharply. Some typical points with positions and function values are labelled for understanding in Figure 3.

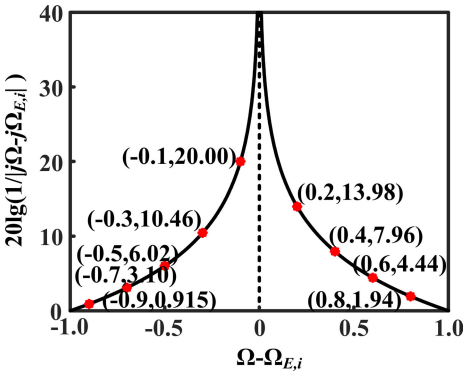

FIGURE 3. Response of the function of $20\lg(1/|j\Omega - j\Omega_{E,i}|)$.

In other words, if an ETZ is placed near to one passband with a higher value of the ripple amplitude difference, it is likely to make a compensation to the ripple amplitude difference between this passband and the others. For example, if an ETZ is placed near to the lth passband with the center frequency $j\Omega_{l0}$, its compensation to the ripple amplitude difference of the lth passband is calculated by the following equation.

$$20\lg\left(\frac{1}{\left|j\Omega_{l0} - j\Omega_{E,i}\right|}\right) \tag{14}$$

With this property, we can estimate how many ETZs are required to be placed at first.

To determine the positions of the ETZs, the following criterion is introduced.

$$\delta_U = \frac{1}{L}\left[\sum_{l=1}^{L} (U_l - E_U)^2\right] \tag{15}$$

where U_l is the ERA of the lth passband as shown in Eq. (10). When the ETZs are added, K_0 in Eq. (10) needs to be changed to K_E. δ_U and E_U represent the variance and the expectation of the ERAs of all passbands. When $\delta_U = 0$, the positions of the ETZs are determined. Eq. (15) could be solved with optimization method. The algorithm solving this optimization problem is the Nelder–Mead algorithm [32]. One important parameter that can affect accuracy by avoiding falling into local extremums is the Usual-Delta. Here, the Usual-Delta is set as 0.03% of the total frequency range from the lower edge frequency of the first passband $j\Omega_{1d}$ to the upper edge frequency of the last passband $j\Omega_{Lu}$, i.e., $[\Omega_{1d}, \Omega_{Lu}]$.

Step 6 (APPLY the Ripple Equality Adjustment): After the ripple amplitude difference adjustment, the ripples in each passband might still be unequal. Then, the ripple equality adjustment should be applied, in which the reflection zeros are shifted. At first, a set of specific frequency points of each passband should be found out, which include the lower edge frequency, the upper edge frequency, and all maximum ripple points. The pth maximum ripple point of the lth passband is denoted by $j\Omega_{M,lp}$, which satisfies the condition of $dK_E(j\Omega)/dj\Omega|_{j\Omega=j\Omega M,lp} = 0$. The variance δ_l of the lth passband is defined as

$$\delta_l = \frac{1}{P_l+2}\left[\sum_{p=1}^{P_l}\left(\left|K_E\left(j\Omega_{M,lp}\right)\right| - E_l\right)^2 + \left(\left|K_E\left(j\Omega_{ld}\right)\right| - E_l\right)^2 + \left(\left|K_E\left(j\Omega_{lu}\right)\right| - E_l\right)^2\right] \tag{16}$$

where E_l is the expectation of $|K_E(j\Omega)|$ at these specific frequency points, and P_l is the number of the maximum ripple points within the lth passband. Then, the total effect is evaluated by summing all δ_l, i.e.,

$$\delta = \sum_{l=1}^{L} \delta_l \tag{17}$$

When $\delta = 0$, the position of the reflection zeros that make the ripples in each passband equal can be determined. Unfortunately, it is not easy to analytically solve Eq. (17). Instead, optimization such as the Nelder–Mead algorithm could be applied.

After the ripple equality adjustment, the ripple amplitude difference of each passband should be 0 and the ripples in each passband could be equal. If no, more than one round of the ripple amplitude difference adjustment and the ripple equality adjustment should be applied until requirement is met.

Step 7 (Determine the Ripple Coefficient ε): Now, the transmission zeros including the specified transmission zeros and the ETZs and the reflection zeros are determined. The modified characteristic function K_E in Eq. (12) is multiplied by ε, the full version of the characteristic function $K(j\Omega)$ is written as

$$K(j\Omega) = \frac{1}{1/\varepsilon}\prod_{l=1}^{L} \frac{\prod_{n=1}^{N_{R,l}} \left(j\Omega - j\Omega_{R,ln}\right)}{\prod_{m=1}^{M_{T,l}} \left(j\Omega - j\Omega_{T,lm}\right)} \prod_{i=1}^{I} \frac{1}{\left(j\Omega - j\Omega_{E,i}\right)} \tag{18}$$

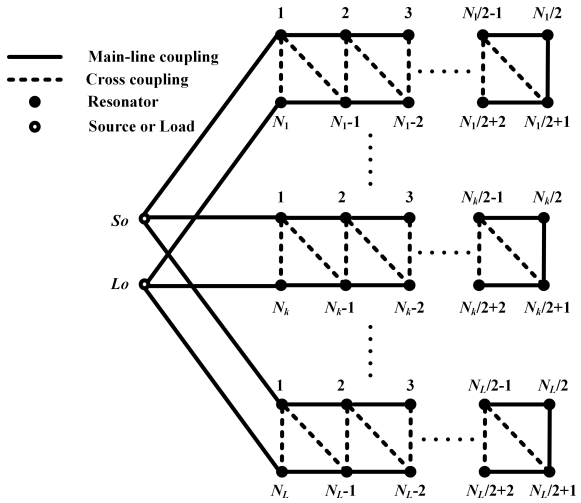

FIGURE 4. L-branch folded topology.

According to Eq. (6), the numerator and the denominator of Eq. (18) correspond to $F(j\Omega)$ and $P(j\Omega)$. By Using Eq. (5), $E(j\Omega)$ is derived. Finally, $S_{21}(j\Omega)$ and $S_{11}(j\Omega)$ are obtained by using Eq. (1) and (2). ε is determined by the return loss at a specified frequency, for example,

$$20\lg\left(|S_{11}\left(j\Omega\right)|\right)|_{\Omega=-1} = RL_1 \tag{19}$$

Up to now, all filtering polynomials are obtained for next-step application. In order to demonstrate the advantages of the proposed RP-FT method, Table 1 list the comparison between it and the work in [2], [5], [7], [13], [27], and [28]. The RP-FT method is featured by flexibly controlling frequency response of MB-BPF.

III. COUPLING MATRIX SYNTHESIS

Section II discusses how to derive the filtering polynomials in detail. By using them, the transversal coupling matrix is obtained as done in [30]. It could be transformed to various topologies for practical realization. In this paper, we consider a specific topology shown in Figure 4, in which there are L branches of the folded topologies for MB-BPF realization. *So*, *Lo*, and *N* represent the source, the load, and the total order of the MB-BPF. In the following, the coupling matrix in the corresponding form will be derived for it.

A. SUBMATRIX FORMATION

According to Figure 4, the transversal coupling matrix denoted as Eq. (20) should be processed to be a specific coupling matrix. For a MB-BPF with L passbands, the diagonal elements (i.e., the self-coupling elements) of the transversal coupling matrix can be divided into L groups according to the closeness of their values. For demonstration, if M_{11} and M_{22} in Eq. (20) are close, then the zone filled with grey can be extracted to form one submatrix as shown in Eq. (21). Eq. (22) shows the general form of one submatrix $[M_l]$.

$$\begin{array}{c|cccccc} & So & 1 & 2 & \cdots & N & Lo \\ So & 0 & M_{So1} & M_{So2} & \cdots & M_{SoN} & 0 \\ 1 & M_{So1} & M_{11} & 0 & 0 & 0 & M_{Lo1} \\ 2 & M_{So2} & 0 & M_{22} & 0 & 0 & M_{Lo2} \\ \vdots & \vdots & \vdots & \vdots & \ddots & \vdots & \vdots \\ N & M_{SoN} & 0 & 0 & \cdots & M_{NN} & M_{LoN} \\ Lo & 0 & M_{Lo1} & M_{Lo2} & \cdots & M_{LoN} & 0 \end{array} \tag{20}$$

$$\begin{array}{c|cccc} & So & 1 & 2 & Lo \\ So & 0 & M_{So1} & M_{So2} & 0 \\ 1 & M_{So1} & M_{11} & 0 & M_{Lo1} \\ 2 & M_{So2} & 0 & M_{22} & M_{Lo2} \\ Lo & 0 & M_{Lo1} & M_{Lo2} & 0 \end{array} \tag{21}$$

$$\begin{array}{c|cccccc} & So & 1 & 2 & \cdots & N_l & Lo \\ So & 0 & M_{l,So1} & M_{l,So2} & \cdots & M_{l,SoN_l} & 0 \\ 1 & M_{l,So1} & M_{l,11} & 0 & 0 & 0 & M_{l,Lo1} \\ 2 & M_{l,So2} & 0 & M_{l,22} & 0 & 0 & M_{l,Lo2} \\ \vdots & \vdots & \vdots & \vdots & \ddots & \vdots & \vdots \\ N_l & M_{l,SoN_l} & 0 & 0 & \cdots & M_{l,N_lN_l} & M_{l,LoN_l} \\ Lo & 0 & M_{l,Lo1} & M_{l,Lo2} & \cdots & M_{l,LoN_l} & 0 \end{array} \tag{22}$$

After the submatrix $[M_l]$ have been extracted, the matrix rotation method is applied to transform it into $\left[M_l^F\right]$ corresponding to one branch of the L-branch folded topology in Figure 4. $\left[M_l^F\right]$ can be further processed by the method in [33] to change the signs of some elements, so that the coupling property can be controlled, then we obtain the final submatrix $\left[M_l^C\right]$. Other submatrices can also be processed like this.

B. QUALITY FACTOR AND COUPLING COEFFICIENT DERIVATION

After obtaining the submatrix $\left[M_l^C\right]$ (where $l = 1, 2, \ldots,$ and L), the resonant frequencies, the quality factors and the coupling coefficients can be derived. Firstly, the resonant frequencies are derived as

$$f_{ln} = \frac{scale}{2\pi} \cdot M_{l,nn}^C + f_0 \tag{23}$$

where $n = 1, 2, \ldots,$ and N_l, respectively. f_{ln} is the resonant frequencies of the nth resonator of the lth branch. $M_{l,nn}^C$ is the nth diagonal element of $\left[M_l^C\right]$.

The center frequency f_l of the lth branch is calculated as

$$f_l = \frac{1}{N_l}\sum_{n=1}^{N_l} f_{ln} \tag{24}$$

where $l = 1, 2, \ldots,$ and L, respectively. The fractional bandwidth FBW_l of the lth branch is

$$FBW_l = \left(f_{Lu} - f_{1d}\right)/f_l \tag{25}$$

The off-diagonal elements in the first (or last) row (or column) of $\left[M_l^C\right]$, i.e, $M_{l,So1}^C$ (or M_{l,LoN_l}^C) are used to calculate

the external quality factors Q_{lS} (or Q_{lL}) [34].

$$Q_{lS} = \frac{1}{\left(M^C_{l,So1}\right)^2 \cdot FBW_l}, \quad Q_{lL} = \frac{1}{\left(M^C_{l,LoN_l}\right)^2 \cdot FBW_l} \tag{26}$$

The other off-diagonal elements in $\left[M^C_l\right]$ that denoted by $M^C_{l,ij}$ $(i = 1, 2, \ldots, N_l; j = 1, 2, \ldots, N_l; i \neq j)$ are used to derive the coupling coefficients $k_{l,ij}$ [34].

$$k_{l,ij} = M^C_{l,ij} \cdot FBW_l \tag{27}$$

IV. SYNTHESIS EXAMPLE

To verify the theory in the previous sections, the RP-FT method is applied to synthesize a quad-band bandpass filter in this section.

A. FILTERING POLYNOMIAL SYNTHESIS

At first, the specifications of the quad-band bandpass filter to be designed are described in the f-domain. The passband number is $L = 4$. The order of each passband is set as $Od_l = 2$. The return loss in each passband is $RL_l = -17$ dB. The center frequencies of the four passbands are (unit: GHz): 5.4098, 7.3900, 9.8294 and 11.8630, respectively. The fractional bandwidths are 3.7%, 2.4%, 2.2% and 1.9%, respectively. Three specified transmission zeros are (unit: GHz): $f_{T,21} = 6.2410$, $f_{T,31} = 8.4721$ and $f_{T,41} = 10.9650$, respectively.

According to Step 1 of the RP-FT method, the first frequency transformation in Eq. (7) is constructed. Here, $f_0 = 8.6420$ GHz, and $scale$=20.942. After this transformation, the specifications are obtained in the Ω-domain: $\Omega_{1d} = -1$, $\Omega_{1u} = -0.9395$, $\Omega_{2d} = -0.4022$, $\Omega_{2u} = -0.3491$, $\Omega_{3d} = 0.3240$, $\Omega_{3u} = 0.3885$, $\Omega_{4d} = 0.9325$, $\Omega_{4u} = 1$, $\Omega_{T,21} = -0.7204$, $\Omega_{T,31} = -0.0510$ and $\Omega_{T,41} = 0.6970$, respectively.

In Step 2, the second frequency transformation is applied. According to Eq. (8), $\Omega_{10} = -0.9700$, $scale^*_1 = 0.0302$, $\Omega_{20} = -0.3757$, $scale^*_2 = 0.0266$, $\Omega_{30} = 0.3562$, $scale^*_3 = 0.0323$, $\Omega_{40} = 0.9663$ and $scale^*_4 = 0.0338$, respectively. Then, the specified transmission zeros in the Ω-domain will be transform into the Ω^*-domain, so that $\Omega^*_{T,21}$, $\Omega^*_{T,31}$ and $\Omega^*_{T,41}$ are obtained.

In Step 3, each passband is considered as a single-band bandpass filter in the Ω^*-domain. For the first passband, there is no specified transmission zero. The specified transmission zero of the second passband is $\Omega^*_{T,21} = -12.9849$, the one of the third passband is $\Omega^*_{T,31} = -12.6279$, and the one of the fourth passband is $\Omega^*_{T,41} = -7.9778$. All the passbands are second-order. Then, the single-band bandpass filter synthesis technique in [30] is applied, and the reflection zeros of each passband is obtained in the Ω^*-domain. The reflection zeros of the first passband are $-j0.7071$ and $j0.7071$, those of the second passband are $-j0.7261$ and $j0.6876$, those of the third passband are $-j0.7267$ and $j0.6870$, and those of the fourth passband are $-j0.7379$ and $j0.6749$, respectively. By using Eq. (8), these reflection zeros are transformed from the Ω^*-domain to the Ω-domain. Accordingly, $\Omega_{R,11} = -0.9911$, $\Omega_{R,12} = -0.9484$, $\Omega_{R,21} = -0.3949$, $\Omega_{R,22} = -0.3574$, $\Omega_{R,31} = 0.3328$, $\Omega_{R,32} = 0.3784$, $\Omega_{R,41} = 0.9414$ and $\Omega_{R,42} = 0.9890$, respectively.

In Step 4, according to Eq. (9), the initial characteristic function of this quad-band bandpass filter is constructed in the Ω-domain, (28) as shown at the bottom of the page.

In Step 5, by using Eq. (10), the ERA of each passband is calculated, i.e., (unit: dB): $U_1 = -51.0683$, $U_2 = -60.0270$, $U_3 = -58.3074$, and $U_4 = -50.1361$, respectively. Because the maximum one of these ERAs is $U_{\max} = -50.1361$ dB. According to Eq. (11), the ripple amplitude difference of each passband is (unit: dB): $\Delta U_1 = 0.9322$, $\Delta U_2 = 9.8909$, $\Delta U_3 = 8.1713$ and $\Delta U_4 = 0$, respectively. Because ΔU_2 and ΔU_3 are much larger than ΔU_1 and ΔU_4, the second and the third passbands need 8∼9 dB compensation for the ripple amplitude difference. According to Figure 3, when the ETZ $j\Omega_{E,i}$ is 0.35 away from the center frequency $j\Omega_{l0}$, a compensation about 8∼9 dB can be made for the ripple amplitude difference. The center frequencies of the second and the third passband are $\Omega_{02} = -0.37565$ and $\Omega_{03} = 0.35625$ respectively, and thus it is appropriate to place one ETZ at 0. The position of this ETZ can be further optimized by Eq. (15). Finally, it is adjusted to $-j0.0469$. Then, the modified characteristic function $K_E(j\Omega)$ is obtained by using Eq. (12), (29) as shown at the bottom of the page.

In Step 6, according to Eq. (17), the positions of the reflection zeros are adjusted to achieve equal ripples in the passbands. The final positions of the reflection zeros are $-j0.9910$, $-j0.9481$, $-j0.3939$, $-j0.3563$, $j0.3329$, $j0.3786$, $j0.9422$ and $j0.9900$, respectively. Then the full version of the

$$K_0(j\Omega) = \frac{(j\Omega + j0.9911)(j\Omega + j0.9484)(j\Omega + j0.3949)(j\Omega + j0.3574)}{(j\Omega - j0.3328)(j\Omega - j0.3784)(j\Omega - j0.9414)(j\Omega - j0.9890)} \Big/ \frac{}{(j\Omega + j0.7204)(j\Omega + j0.0510)(j\Omega - j0.6970)} \tag{28}$$

$$K_E(j\Omega) = \frac{(j\Omega + j0.9911)(j\Omega + j0.9484)(j\Omega + j0.3949)(j\Omega + j0.3574)}{(j\Omega - j0.3328)(j\Omega - j0.3784)(j\Omega - j0.9414)(j\Omega - j0.9890)} \Big/ \frac{}{(j\Omega + j0.7204)(j\Omega + j0.0510)(j\Omega - j0.6970)(j\Omega + j0.0469)} \tag{29}$$

TABLE 1. Performance comparison of transfer function.

	[2]	[5]	[7]	[13]	[27]	[28]	This work
Ripples in each passband equal?	✓	✓	✓	✓	✓	✓	✓
Order of each passband controllable?	×	✓	✓	✓	×	×	✓
Bandwidth of each passband adjustable?	✓	✓	✓	✓	✓	✓	✓
Return loss in each passband controllable?	×	×	✓	×	×	×	✓
Center frequency of each passband adjustable?	✓	✓	×	✓	✓	✓	✓
Number of bands controllable?	✓	✓	✓	✓	✓	✓	✓
Transmission zeros adjustable?	×	✓	✓	✓	×	×	✓

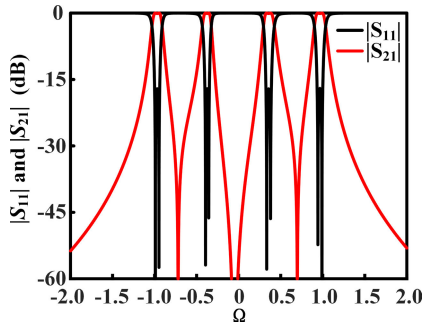

FIGURE 5. Synthesized response of the quad-band bandpass filter in the Ω-domain.

characteristic function $K(\Omega)$ is (30), as shown at the bottom of the page.

In Step 7, Eq. (19) is used. When $RL_1 = -17$ dB, ε calculated to be 46.5797. Then, S_{21} can be found as

$$S_{21}(s) = j0.02147 \frac{\begin{array}{c}(s+j0.7204)(s+j0.0510)\\(s-j0.6970)(s+j0.0469)\end{array}}{\begin{array}{l}(s+0.0387+j1.0131)(s+0.0358+j0.9259)\\(s+0.0370+j0.4131)(s+0.0288+j0.3372)\\(s+0.0362-j0.3095)(s+0.0435-j0.4022)\\(s+0.0422-j1.0144)(s+0.0403-j0.9176)\end{array}} \quad (31)$$

The response of this quad-band bandpass filter in the Ω-domain is shown in Figure 5. The center frequencies are: −0.9693, −0.3755, 0.3563 and 0.9660, respectively. The in-band return loss are −17 dB as required. The four transmission zeros are 0.7204, 0.0510, −0.0469 and 0.6970, respectively.

B. COUPLING MATRIX SYNTHESIS

The transversal coupling matrix is synthesized and presented in Eq. (32), as shown at the bottom of the next page. According to Section III, it can be divided into four submatrices, i.e., $[M_l]$ (where $l = 1, 2, 3,$ and 4, respectively). The matrix rotation method in [30] is used to transform $[M_l]$ to the folded topology, then $\left[M_l^F\right]$ is obtained and presented in Eq. (33), as shown at the bottom of the next page. In these submatrices, $M_{l,Lo1}^F \ll M_{l,Lo2}^F$. For simplification, $M_{l,Lo1}^F$ is neglected and set to be 0. After applying the sign shift method in [33], the final submatrix $\left[M_l^C\right]$ is presented in Eq. (34), as shown at the bottom of the next page. The 4-branch folded topology for realizing the quad-band bandpass filter is shown in Figure 6.

By bringing $f_0 = 8.642$ GHz and $scale$=20.942 into Eq. (23), the resonant frequencies in Figure 6 are determined as (unit: GHz): $f_{11} = 5.4037$, $f_{12} = 5.4103$, $f_{21} = 7.4418$, $f_{22} = 7.4695$, $f_{31} = 9.9102$, $f_{32} = 9.8792$, $f_{41} = 11.8920$, and $f_{42} = 11.8813$, respectively. According to Eq. (24), the center frequencies of these four branches are (unit: GHz): $f_1 = 5.407$, $f_2 = 7.456$, $f_3 = 9.895$, and $f_4 = 11.887$, respectively. By using Eq. (25), the fractional bandwidths of these four branches are: $FBW_1 = 123.28\%$, $FBW_2 = 89.41\%$, $FBW_3 = 67.37\%$ and $FBW_4 = 56.08\%$, respectively. Then, the external quality factors are determined by Eq. (26), and they are: $Q_{1S} = 19.5310$, $Q_{1L} = 19.5401$, $Q_{2S} = 28.2725$, $Q_{2L} = 28.5029$, $Q_{3S} = 45.4302$, $Q_{3L} = 46.1339$, $Q_{4S} = 47.5813$ and $Q_{4L} = 47.6458$, respectively. The coupling coefficients determined by Eq. (27) are: $k_{112} = 0.0590$, $k_{212} = 0.0409$, $k_{312} = -0.0254$ and $k_{412} = -0.0242$, respectively.

V. MICROSTRIP REALIZATION AND MEASUREMENT

In order to verify the RP-FT method, this section present a microstrip realization to realize the quad-band bandpass filter discussed in Section IV. The design detail is presented for verification.

A. MICROSTRIP REALIZATION

We propose a microstrip realization in Figure 7 to realize the 4-branch folded topology in Figure 6. It contains four

$$K(j\Omega) = \frac{1}{1/\varepsilon} \frac{(j\Omega+j0.9910)(j\Omega+j0.9481)(j\Omega+j0.3939)(j\Omega+j0.3563)}{(j\Omega-j0.3329)(j\Omega-j0.3786)(j\Omega-j0.9422)(j\Omega-j0.9900)} \quad (30)$$

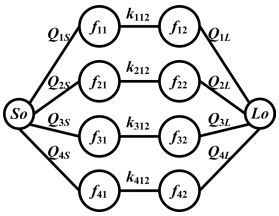

FIGURE 6. The 4-branch folded topology for the quad-band bandpass filter.

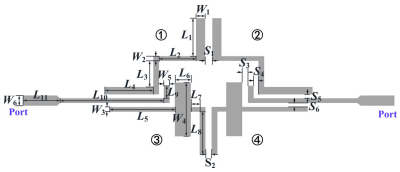

FIGURE 7. Microstrip realization of the quad-band bandpass filter.

resonators to provide eight resonances for operation. The fundamental resonance f_{11} of Resonator ① is coupled to that the fundamental resonance f_{12} of Resonator ② to form the first passband with the center frequency f_1 at 5.4070 GHz. Their first harmonics denoted by f_{41} and f_{42} are coupled to form the fourth passband with the center frequency f_4 at 11.8867 GHz. The fundamental resonance f_{21} of Resonator ③ is coupled to that the fundamental resonance f_{22} of Resonator ④ to form the second passband with the center frequency f_2 at 7.4556 GHz. Their first harmonics denoted by f_{31} and f_{32} to form the third passband with the center frequency f_3 at 9.8946 GHz.

By using the quality factors and the coupling coefficients derived in Section IV, the initial dimensions of the microstrip construction in Figure 7 can be determined. The procedure follows that described in [34]. After full-wave optimization, the final dimensions are (unit: mm): $L_1 = 4.10$, $L_2 = 3.25$, $L_3 = 2.82$, $L_4 = 4.25$, $L_5 = 5.75$, $L_6 = 1.4$, $L_7 = 0.78$, $L_8 = 4.63$, $L_9 = 1.35$, $L_{10} = 9.10$, $L_{11} = 1.805$, $W_1 = 0.80$, $W_2 = 0.50$, $W_3 = 0.50$, $W_4 = 5.80$, $W_5 = 0.50$, $W_6 = 1.10$, $S_1 = 0.33$, $S_2 = 0.21$, $S_3 = 0.81$, $S_4 = 0.12$, $S_5 = 0.12$ and $S_6 = 0.13$, respectively.

Figure 8 depicts the comparison between the synthesis result and the simulation result of the microstrip filter in Figure 7. The simulated center frequencies are 5.40, 7.39, 9.81 and 11.83 GHz, respectively. The fractional bandwidths are 3.7%, 2.2%, 1.9% and 1.7%, respectively. The in-band return losses are 16.0, 32.0, 18.0, and 19.0 dB, respectively. The insertion losses are 1.43, 1.56, 2.16, and

0	-0.1457	0.1394	-0.1343	0.1425	-0.1355	0.1468	0.1197	-0.1342	0
-0.1457	-1.0185	0	0	0	0	0	0	0	0.1457
0.1394	0	1.0167	0	0	0	0	0	0	0.1394
-0.1343	0	0	0.9303	0	0	0	0	0	0.1343
0.1425	0	0	0	-0.9227	0	0	0	0	0.1425
-0.1355	0	0	0	0	0.4135	0	0	0	0.1355
0.1468	0	0	0	0	0	-0.4017	0	0	0.1468
0.1197	0	0	0	0	0	0	0.3382	0	0.1197
-0.1342	0	0	0	0	0	0	0	-0.3102	0.1342
0	0.1457	0.1394	0.1343	0.1425	0.1355	0.1468	0.1197	0.1342	0

(32)

$[M_1^F]$			
0	-0.2038	0	0
-0.2038	-0.9716	-0.0479	0.0044
0	-0.0479	-0.9696	0.2037
0	0.0044	0.2037	0

$[M_2^F]$			
0	0.1989	0	0
0.1989	-0.3601	-0.0456	0.0179
0	-0.0456	-0.3518	0.1981
0	0.0179	0.1981	0

$[M_3^F]$			
0	0.1808	0	0
0.1808	0.3805	-0.0373	-0.0223
0	-0.0373	0.3712	0.1794
0	-0.0223	0.1794	0

$[M_4^F]$			
0	-0.1936	0	0
-0.1936	0.9751	-0.0432	-0.0071
0	-0.0432	0.9719	0.1935
0	-0.0071	0.1935	0

(33)

$[M_1^C]$			
0	0.2038	0	0
0.2038	-0.9716	0.0479	0
0	0.0479	-0.9696	0.2037
0	0	0.2037	0

$[M_2^C]$			
0	-0.1989	0	0
-0.1989	-0.3601	0.0456	0
0	0.0456	-0.3518	0.1981
0	0	0.1981	0

$[M_3^C]$			
0	0.1808	0	0
0.1808	0.3805	-0.0373	0
0	-0.0373	0.3712	0.1794
0	0	0.1794	0

$[M_4^C]$			
0	0.1936	0	0
0.1936	0.9751	-0.0432	0
0	-0.0432	0.9719	-0.1935
0	0	-0.1935	0

(34)

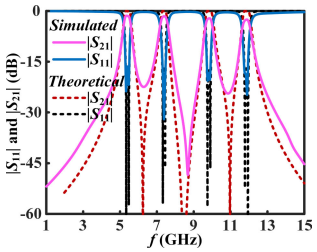

FIGURE 8. Theoretical result and the full-wave simulation result.

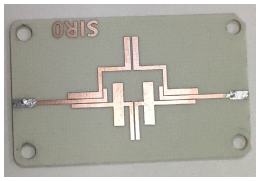

FIGURE 9. Photo of the fabricated microstrip quad-band bandpass filter example.

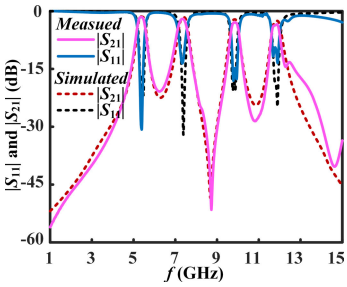

FIGURE 10. Simulated and measured results of the fabricated microstrip quad-band bandpass filter example.

2.54 dB, respectively. The simulation results coincide very well with the synthesized ones except that one transmission zero between the first two passbands and the one between the last two passbands are not so obvious. This is because that the susceptance slope of each resonator in the theory is a constant in all frequency range but that of each microstrip resonator is not.

B. MEASUREMENT

The microstrip quad-band bandpass filter was fabricated and measured. The photo of the fabricated filter is shown in Figure 9. The measured and simulated S parameters are depicted in Figure 10. The measured center frequencies are 5.39, 7.36, 9.85 and 11.81 GHz, respectively. The fractional bandwidths are 3.0%, 1.4%, 1.6% and 1.8% respectively. The in-band return losses are 30.0, 13.0, 15.0, and 10.0 dB, respectively. The insertion losses are 1.52, 2.00, 2.95, and 3.60 dB respectively. The measured results coincide well with the simulated ones except that the measured return losses of the second and the fourth passband deteriorate to some extent. As analysis shows, the response of the filter is sensitive to the variation of the dimension parameter L_7. The required value of L_7 is 0.78 mm. However, fabrication precision unfortunately causes minor deviation. We found out that the simulated response with $L_7 = 0.75$ mm is very close to the measured response.

VI. CONCLUSION

As a very important circuit component for frequency selection, MB-BPF is receiving much attention. But, to design a MB-BPF is still very challenging. In this paper, a hybrid approach is proposed for the synthesis of MB-BPF, which is named the RP-FT method. It includes two main parts, i.e., the rough prototype construction and the fine tuning optimization. The rough prototype construction contains necessary information of the MB-BPF to be synthesized, which efficiently narrow scope for the fine tuning optimization. In addition, the Nelder–Mead algorithm is utilized for fine tuning, which can accelerate search process. The proposed RP-FT method is featured by fast convergence and flexibly controlling the performance of a MB-BPF such as passband number, performance of each passband, transmission zeros, etc.

REFERENCES

[1] J. Lee and K. Sarabandi, "A synthesis method for dual-passband microwave filters," *IEEE Trans. Microw. Theory Techn.*, vol. 55, no. 6, pp. 1163–1170, Jun. 2007.
[2] J. Lee and K. Sarabandi, "Design of triple-passband microwave filters using frequency transformations," *IEEE Trans. Microw. Theory Techn.*, vol. 56, no. 1, pp. 187–193, Jan. 2008.
[3] G. Li, B. Wu, X.-W. Dai, and C.-H. Liang, "Design techniques for asymmetric dual-passband filters," *J. Electromagn. Waves Appl.*, vol. 22, nos. 2–3, pp. 375–383, Jan. 2008.
[4] S. Awasthi, A. Biswas, and M. J. Akhtar, "Synthesis of symmetric and asymmetric triple-stopband microwave filter using frequency transformation," in *Proc. URSI Int. Symp. Electromagn. Theory (EMTS)*, Hiroshima, Japan, 2013, pp. 485–488.
[5] Y.-T. Kuo, J.-C. Lu, C.-K. Liao, and C.-Y. Chang, "New multiband coupling matrix synthesis technique and its microstrip implementation," *IEEE Trans. Microw. Theory Techn.*, vol. 58, no. 7, pp. 1840–1850, Jul. 2010.
[6] X. Chen, L. Zhang, C. Xu, Z. Zheng, and X. Jiang, "Dual-band filter synthesis based on two low-pass prototypes," *IEEE Microw. Wireless Compon. Lett.*, vol. 27, no. 10, pp. 903–905, Oct. 2017.
[7] X. Chen, "Synthesis of multi-band filters based on multi-prototype transformation," *IET Microw., Antennas Propag.*, vol. 15, no. 2, pp. 103–114, Feb. 2021.
[8] Y. Zhang, K. A. Zaki, J. A. Ruiz-Cruz, and A. E. Atia, "Analytical synthesis of generalized multi-band microwave filters," in *IEEE MTT-S Int. Microw. Symp. Dig.*, Honolulu, HI, USA, Jun. 2007, pp. 1273–1276.
[9] Z. Liang-Yu and L. Sheng-Xian, "A new synthesis method for equiripple dual-passband microwave filters," in *Proc. IEEE Int. Conf. Microw. Technol. Comput. Electromagn.*, Beijing, China, May 2011, pp. 114–117.
[10] S. Bila, R. Cameron, P. Lenoir, V. Lunot, and F. Seyfert, "Chebyshev synthesis for multi-band microwave filters," in *IEEE MTT-S Int. Microw. Symp. Dig.*, San Francisco, CA, USA, Jun. 2006, pp. 1221–1224.
[11] V. Lunot, S. Bila, and F. Seyfert, "Optimal synthesis for multi-band microwave filters," in *IEEE MTT-S Int. Microw. Symp. Dig.*, Honolulu, HI, USA, Jun. 2007, pp. 115–118.
[12] V. Lunot, F. Seyfert, S. Bila, and A. Nasser, "Certified computation of optimal multiband filtering functions," *IEEE Trans. Microw. Theory Techn.*, vol. 56, no. 1, pp. 105–112, Jan. 2008.
[13] E. Musonda, R. A. Paradkar, I. C. Hunter, and R. Parry, "Synthesis of multiband filters by linear optimization," *IEEE Trans. Microw. Theory Techn.*, vol. 67, no. 12, pp. 4764–4772, Dec. 2019.
[14] R. J. Cameron, M. Yu, and Y. Wang, "Direct-coupled microwave filters with single and dual stopbands," *IEEE Trans. Microw. Theory Techn.*, vol. 53, no. 11, pp. 3288–3297, Nov. 2005.
[15] Y. Mo, K. Song, and Y. Fan, "Miniaturized triple-band bandpass filter using coupled lines and grounded stepped impedance resonators," *IEEE Microw. Wireless Compon. Lett.*, vol. 24, no. 5, pp. 333–335, May 2014.
[16] L. Gao, X. Y. Zhang, X.-L. Zhao, Y. Zhang, and J.-X. Xu, "Novel compact quad-band bandpass filter with controllable frequencies and bandwidths," *IEEE Microw. Wireless Compon. Lett.*, vol. 26, no. 6, pp. 395–397, Jun. 2016.

[17] S.-W. Wong, Z.-C. Guo, J.-Y. Lin, L. Zhu, and Q. Zhang, "Triple-mode and triple-band cavity bandpass filter on triplet topology with controllable transmission zeros," *IEEE Access*, vol. 6, pp. 29452–29459, 2018.
[18] H.-W. Xie, K. Zhou, C.-X. Zhou, and W. Wu, "Substrate-integrated waveguide triple-band bandpass filters using triple-mode cavities," *IEEE Microw. Theory Techn.*, vol. 66, no. 6, pp. 2967–2977, Jun. 2018.
[19] Y. Xie, F.-C. Chen, Q.-X. Chu, and Q. Xue, "Dual-band coaxial filter and diplexer using stub-loaded resonators," *IEEE Trans. Microw. Theory Techn.*, vol. 68, no. 7, pp. 2691–2700, Jul. 2020.
[20] G. Macchiarella and S. Tamiazzo, "Design techniques for dual-passband filters," *IEEE Trans. Microw. Theory Techn.*, vol. 53, no. 11, pp. 3265–3271, Nov. 2005.
[21] X.-P. Chen, K. Wu, and Z.-L. Li, "Dual-band and triple-band substrate integrated waveguide filters with Chebyshev and quasi-elliptic responses," *IEEE Trans. Microw. Theory Techn.*, vol. 55, no. 12, pp. 2569–2578, Dec. 2007.
[22] H. Di, B. Wu, X. Lai, and C.-H. Liang, "Synthesis of cross-coupled triple-passband filters based on frequency transformation," *IEEE Microw. Wireless Compon. Lett.*, vol. 20, no. 8, pp. 432–434, Aug. 2010.
[23] A. Garcia-Lamperez and M. Salazar-Palma, "Single-band to multiband frequency transformation for multiband filters," *IEEE Trans. Microw. Theory Techn.*, vol. 59, no. 12, pp. 3048–3058, Dec. 2011.
[24] S. A. Shakib, V. Sekar, and K. Entesari, "A compact triple-band bandpass filter based on half-mode substrate integrated waveguides," in *Proc. 42nd Eur. Microw. Conf.*, Amsterdam, The Netherlands, Oct. 2012, pp. 116–119.
[25] P. Ma, B. Wei, J. Hong, Z. Xu, X. Guo, B. Cao, and L. Jiang, "A design method of multimode multiband bandpass filters," *IEEE Trans. Microw. Theory Techn.*, *IEEE Trans. Microw. Theory Techn.*, vol. 66, no. 6, pp. 2791–2799, Jun. 2018.
[26] Y. Wu, E. Fourn, P. Besnier, and C. Quendo, "Direct synthesis of quad-band band-pass filter by frequency transformation methods," in *Proc. 49th Eur. Microw. Conf. (EuMC)*, Paris, France, Oct. 2019, pp. 196–199.
[27] Y. Wu, E. Fourn, P. Besnier, and C. Quendo, "Direct synthesis of multi-band bandpass filters with generalized frequency transformation methods," *IEEE Trans. Microw. Theory Techn.*, vol. 69, no. 8, pp. 3820–3831, Aug. 2021.
[28] M. Khaliel, J. Wen, A. Prokscha, A. El-Awamry, A. Fawky, and T. Kaiser, "Synthesis and realization of multiband bandpass filters based on frequency transformation for the encoding of chipless RFID tags," in *Proc. IEEE-APS Topical Conf. Antennas Propag. Wireless Commun. (APWC)*, Honolulu, HI, USA, Aug. 2021, pp. 184–188.
[29] Y. Wu, K. Ma, and Y. Wang, "Coupling matrix design of compact multi-band cascaded trisection bandpass filters," *IEEE Trans. Circuits Syst. II, Exp. Briefs*, vol. 69, no. 6, pp. 2762–2766, Jun. 2022.
[30] R. J. Cameron, C. M. Kudsia, and R. R. Mansour, *Microwave Filters for Communication Systems: Fundamentals, Design, and Applications*, 2nd ed. Hoboken, NJ, USA: Wiley, 2018.
[31] R. Wu, X. Tang, J. He, Y. Cao, L. Xiao, and F. Xiao, "The DST-O method for multiband IIR filter," *Circuits, Syst., Signal Process.*, pp. 1–8, Aug. 2022.
[32] J. C. Lagarias, J. A. Reeds, M. H. Wright, and P. E. Wright, "Convergence properties of the Nelder–Mead simplex method in low dimensions," *SIAM J. Optim.*, vol. 9, no. 1, pp. 112–147, 1998.
[33] S. Qian, G. Brand, J. Hong, and P. Meyer, "The design of miniature multilayer bandpass filters with mixed couplings," *IEEE Trans. Microw. Theory Techn.*, vol. 61, no. 12, pp. 4072–4078, Dec. 2013.
[34] J.-S. G. Hong and M. J. Lancaster, *Microstrip Filters for RF/Microwave Applications*. Hoboken, NJ, USA: Wiley, 2004.

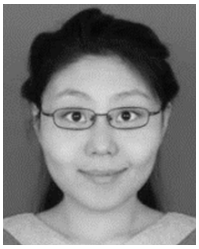

RIHAN WU (Member, IEEE) was born in Baotou, China, in 1988. She received the B.S. degree in electronic and information engineering from the North University of China, Shanxi, in 2011, and the M.S. degree in electronic and communication engineering from Inner Mongolia University, Inner Mongolia, in 2015. She is currently pursuing the Ph.D. degree in electromagnetic field and microwave technology with the University of Electronic Science and Technology of China (UESTC), Chengdu. Her research interests include electromagnetic field theory research and microwave passive circuit component design.

JUNLING HE was born in Yining, Xinjiang, China. He received the B.S. and M.S. degrees from Sichuan University, Chengdu, China, in 2016 and 2021, respectively. He is currently pursuing the Ph.D. degree in electronic science and technology with the University of Electronic Science and Technology of China (UESTC), Chengdu. His research interests include microwave passive circuit and tunable circuit and antenna.

XIAOHONG TANG (Member, IEEE) received the B.S. and Ph.D. degrees from the University of Electronic Science and Technology of China (UESTC), Chengdu, in 1983 and 1990, respectively. He is currently a full-time Professor. His research interests include microwave/millimeter circuit and system design.

ZONGQI CAI was born in Fujian, China, in 1991. He received the Ph.D. degree from the School of Electronic Science and Engineering, University of Electronic Science and Technology of China (UESTC), Chengdu, in 2020. He was a Visiting Scholar with UTS, from 2017 to 2019. He is currently an Engineer with the National Key Laboratory of Science and Technology on Reliability Physics and Application of Electronic Component, China Electronic Product Reliability and Environmental Testing Research Institute. His research interests include design and measurement of RF/microwave low phase noise oscillator/amplifier/filter/Doppler radar, electromagnetic compatibility, failure analysis, and reliability of microwave components.

LIKANG XIAO is currently a Senior Engineer with the Southwest Institute of Applied Magnetics, Sichuan, China. His research interests include ferrite analysis and application and microwave circuit component design.

FEI XIAO (Member, IEEE) received the M.Sc. and Ph.D. degrees from the University of Electronic Science and Technology of China (UESTC), in 2002 and 2005, respectively. From October 2009 to October 2010, he was a Visiting Researcher at the KTH Royal Institute of Technology, Sweden. From October 2015 to March 2016, he was a Visiting Researcher at the University of Birmingham, U.K. He is currently a Professor with UESTC. He has authored more than 120 journal and conference papers and holds 30 authorized patents. His research interests include filter synthesis, microwave passive components design, and computational electromagnetics.